Journal of Composite Materials

http://jcm.sagepub.com

Limiting Mechanisms of Mode I Interlaminar Toughening of Composites Reinforced with Aligned Carbon Nanotubes

Joaquín Blanco, Enrique J. García, Roberto Guzmán de Villoria and Brian L. Wardle

Journal of Composite Materials 2009; 43; 825
DOI: 10.1177/0021998309102398

The online version of this article can be found at:
http://jcm.sagepub.com/cgi/content/abstract/43/8/825

Published by:
SAGE
http://www.sagepublications.com

On behalf of:
American Society for Composites

Limiting Mechanisms of Mode I Interlaminar Toughening of Composites Reinforced with Aligned Carbon Nanotubes

JOAQUÍN BLANCO, ENRIQUE J. GARCÍA, ROBERTO GUZMÁN DE VILLORIA AND BRIAN L. WARDLE*
Department of Aeronautics and Astronautics, Massachusetts Institute of Technology, Cambridge, MA-02139, USA

ABSTRACT: Analytical models are presented for the Mode I interlaminar fracture of laminated composites reinforced with aligned carbon nanotubes (CNTs). The models are based on the crack-closure technique for fiber bridging, where the aligned CNTs enhance toughness mechanistically through either pullout (frictional sliding) from the matrix or sword-in-sheath sliding. The models are independent of the scale of reinforcement and demonstrate significant enhanced toughening for nanoscale reinforcement (CNTs) as opposed to typical mm-scale reinforcements (stitches and Z-pins). Complete analytical expressions for crack-growth resistance ($G_R(\Delta a)$) are obtained including normalized closed-form expressions for steady-state toughness for any scale of z-direction fiber reinforcement. The model is verified by comparison to previous experimental results for Z-pins and also aligned CNTs, and is used to define regimes where the competing mechanisms of toughening are operative. CNT strength is a key parameter limiting toughness enhancement in the frictional pullout mechanism.

KEY WORDS: fracture toughness, Nanomaterials, CNT, Mode I delamination, crack growth resistance, nanostitching, pullout, sword-in-sheath.

INTRODUCTION

COMPOSITE LAMINATES CONTAIN matrix-rich regions at ply interfaces that can reduce their overall performance. Delamination and matrix cracking between plies are the dominant modes of damage, and therefore responsible for the reduction of properties in the direction normal to the plane which can lead to in-plane reductions as well. In recent years, several different solutions have attempted to overcome this limitation: 3D-braiding, weaving, stitching, and z-pinning have all been considered [1]. In all these solutions to date, the reinforcement comprises micron-diameter advanced fibers in tow or yarn form, with cross-sections of the order of millimeters. All these processes increase to some extent the

*Author to whom correspondence should be addressed. E-mail: wardle@mit.edu
Figure 1 appears in color online: http://jcm.sagepub.com

0021-9983/09/08 0825–17 $10.00/0 DOI: 10.1177/0021998309102398

through-thickness mechanical properties of laminated composite materials, but also reduce the laminate's performance in the in-plane directions [1–8]. In state-of-the-art stitching and z-fiber reinforcement [1], through-thickness properties generally increase significantly with the number of 'stitches' (characterized by stitch spacing/density or volume fraction) [1,9–11], while in-plane properties are increasingly degraded as 'stitch' density increases due to insertion damage and interaction [12,13]. As an example, tensile and compressive strength decreases by ~30% for z-fiber reinforcement [13], and substantial reductions are generally concluded for stitching, with the most pronounced reductions observed with prepreg materials [12].

A possible method to increase a composite's resistance to delamination without compromising the in-plane properties is the use of carbon nanotubes (CNTs) or other nanostructures at the interface between plies that would not only improve the mechanical properties across the interface, but also help to reduce crack propagation by bridging the two plies across the interface. Unlike the substantial degradation of in-plane properties observed for stitching and z-pinning, there is conceivably no loss of in-plane properties with an 'interlaminar nanostitch' due to the absence of fabrication damage to the plies being joined. Recent work using randomly oriented carbon nanofibers and CNTs placed between plies using different techniques (unaligned CNTs mixed between tows [14], electrophoresis [15], additional CNT/epoxy layer [16], and spraying [17]) have shown limited enhanced reinforcement (to a maximum of ~30% for the electrophoresis deposited CNTs). CNTs in these prior works are unaligned, a characteristic likely important for both mechanical and other interface properties. Vertically aligned CNTs (VACNTs) have been incorporated into the interlaminar region of aerospace-grade prepreg systems to create 'nanostitches' [18]. Such a hybrid system has three parts: advanced (carbon) fibers, an aerospace-grade polymer resin, and aligned CNTs oriented perpendicular to the ply surface (i.e., in the z-direction) to reinforce the laminate's interlaminar properties. The interlaminar 'nanostitch' (Figure 1) motivates the analytical development because VACNTs are used at the interface as idealized in the model described subsequently.

The model developed here treats the CNTs as mechanical reinforcing elements and, therefore, can be applied to any scale of reinforcement. The model allows scale effects, due to the high surface-to-volume ratio of the CNTs as the reinforcement diameter approaches nanometer scales, to be quantitatively investigated. Results from pullout experiments of individual CNTs from polymer matrices [19,20] demonstrated a mechanical response similar to the pullout process of a z-pin or stitch from the polymer [21]. The reinforcement mechanism of the VACNTs was considered analogous to the one demonstrated by the z-pins: the reinforcing pins (here VACNTs) are perpendicularly embedded into the matrix-rich region at the interface between plies. If delamination occurs (as in a typical Mode I fracture) the pins (VACNTs) bridge the crack between the plies until they are completely pulled out (Figure 2). This bridging effect resists crack propagation, increasing the fracture toughness due to frictional sliding of the CNTs during pullout. The analysis also considers the mechanism of sword-in-sheath pullout, where the outer shell of a multi-walled CNT (MWCNT) remains attached to the polymer and the inner tube(s) pull out of this outer tube following fracture of the inner tube(s). Here, a closed-form solution for the reinforcing effect of VACNTs acting as interlaminar 'nanostitches' or z-pins is presented. A similar model using numerical integration of an approximate stress-intensity factor solution for a point load has treated the same problem from a parametric perspective [22], rather than in closed-form using an energy-based approach as developed herein.

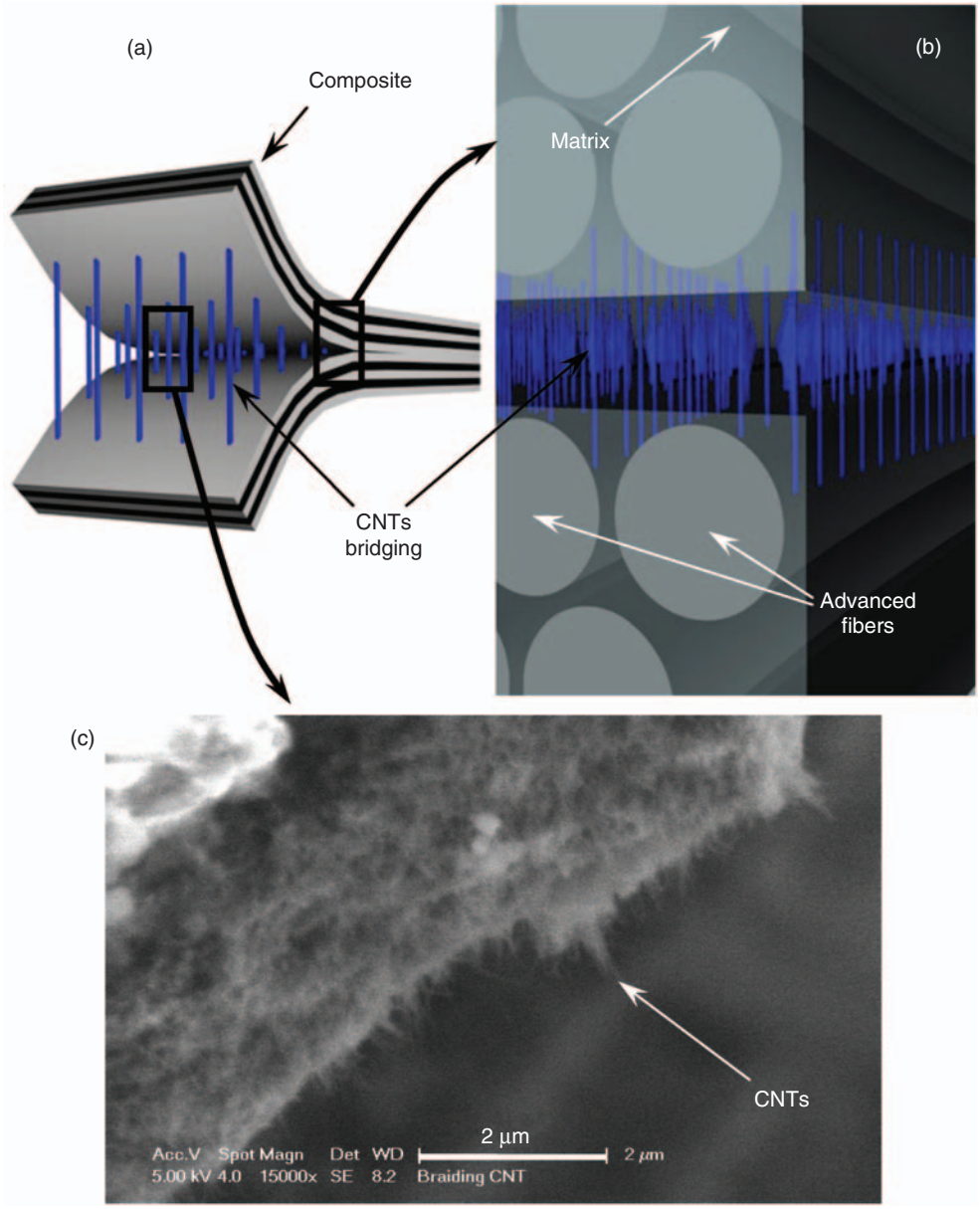

Figure 1. *CNT-reinforced interlaminar architecture: (a) Idealized VACNTs placed in between two plies of a laminated composite. (b) Close-up of the crack, showing idealized VACNTs bridging the crack between the two plies. Illustrations are not to scale. (c) SEM image of crack surface after Mode I fracture testing of a nanostitched AS4/8552 laminate with CNT bundles clearly visible.*

Other work on short fiber composite bridging has adopted an energy-based approach similar to that presented here, but did not consider aligned z-direction reinforcement [23,24].

The model here considers reinforcing elements oriented perpendicular to the laminate interlaminar region (valid for nanostitches, z-pins, and stitches) and would need to be adapted to treat reinforcing CNTs that are not perpendicular to the midplane, as in recent

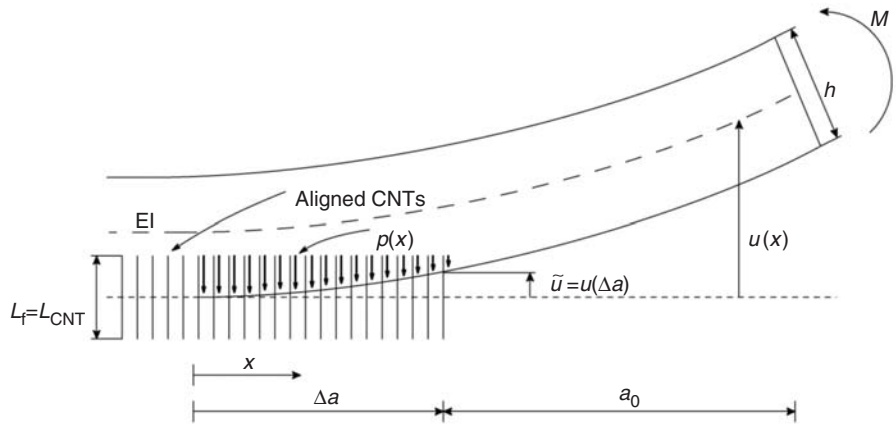

Figure 2. *Illustration of the aligned fiber/CNT-bridged Mode I specimen.*

experimental work where CNTs are grown on fibers at the ply interface [25] and within woven fiber cloth [26].

CLOSED FORM SOLUTIONS FOR MODE I ALIGNED-CNT BRIDGING TOUGHENING IN STEADY-STATE

For the derivation of the closed form solution for steady-state, a double cantilever beam (DCB) specimen with CNTs perpendicularly bridging the crack was considered as in Figure 2. This process is mainly characterized by two fracture parameters, G_0 (initial toughness) and G_{SS} (steady-state toughness including bridging). In a standard R-curve for a specimen undergoing such toughening G_R increases from G_0 to G_{SS} due to the bridging pins that are pulled out from the matrix. Bridging reaches steady-state when the first pin is completely pulled out, and the resistance remains constant during further crack advance.

As the R-curve depends on the thickness of the specimen, but not G_{ss} [27], the analysis will focus on the steady state propagation and present the ratio G_{ss}/G_0 as the main parameter of fracture toughness improvement. The balance of energy when the crack propagates is conveniently expressed through application of the J-integral [27,28]:

$$G_R(\Delta a) = G_0 + 2\int_0^{\tilde{u}} p(x)\mathrm{d}u \tag{1}$$

where $\tilde{u}$ is the end of the crack opening of the bridged zone and $p(x)$ is the closure traction stress due to the action of the pins (here, CNTs) as shown in Figure 2. For steady state, $\tilde{u}$ is known and equals $L_f/2$ (L_f being the reinforcing fiber length, $L_f = L_{CNT}$ for the case of nanostitches, where L_{CNT} is the average height of the VACNTs), assuming the pins are completely pulled out from both sides of the crack, a nonconservative assumption representing an upper bound. The bridging traction in Equation (1) can be due to either simple CNT pullout from the matrix (interfacial shear stress – IFSS) or due to sword-in-sheath pullout of a MWCNT, where the outer CNT wall is broken and the inner remaining tubes pull out of the external CNT wall which remains attached to the matrix [29,30].

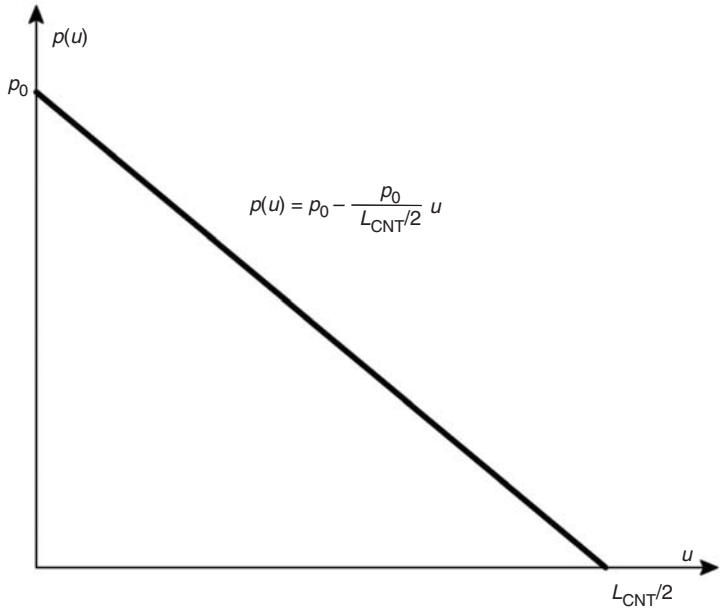

Figure 3. *Linear bridging law for pullout of CNTs.*

In the sword-in-sheath mechanism, frictional sliding occurs as in the pullout IFSS mechanism. Both types of toughening are modeled in the sections that follow.

Pullout Mechanism

To capture bridging due to pullout, the Dugdale model [31] is employed, which in its generalized form uses a homogenized bridging zone law of continuously distributed nonlinear springs. Owing to the nature of the bridging, only a linear and softening response will be used (Figure 3). Here, the closure traction p depends on the separation u at each point in the bridged zone ($p = p(u)$). In the case of linear bridging:

$$p(u) = \alpha_p + \beta_p u \quad \text{for } u < \tilde{u} \tag{2}$$

$$G_R = G_0 + 2\int_0^{\tilde{u}} (\alpha_p + \beta_p u)\, \mathrm{d}u = G_0 + \frac{1}{\beta_p}\left[(\alpha_p + \beta_p \tilde{u})^2 - \alpha_p^2\right] \tag{3}$$

Using a simple pullout model, the bridging law in Equation (2) can be expressed as a function of the relevant parameters of the problem (CNT volume fraction, CNT length, CNT radius, and frictional force). Here, CNT volume fraction refers to the local volume fraction of CNTs in the interlaminar region, i.e., the area fraction of VACNTs in the plane normal to the z-direction. The bridging force, $F(x)$, acting on an infinitesimal element, $\mathrm{d}x$, at distance x from the crack tip can be expressed as:

$$F(x) = \begin{cases} 2\pi r n \tau_c \left(\dfrac{L_{CNT}}{2} - u(x)\right) & 0 < u(x) < \dfrac{L_{CNT}}{2} \\ 0 & \dfrac{L_{CNT}}{2} < u(x) \end{cases} \tag{4}$$

where n is the number of CNTs in dx, τ_c is the coefficient of friction of the CNT 'fiber' being pulled out (equal to IFSS of the CNT in the polymer), and r and L_{CNT} are, respectively, the radius and the length of the CNTs (more generally L_{CNT} would be the length of the bridging fiber, L_f). The volume fraction of the CNTs is $v_{CNT} = n\pi r^2/b\mathrm{d}x$, where b is the width of the specimen. Using this definition in Equation (4), the bridging stress on the crack face can be expressed as:

$$p(x) = \frac{F(x)}{b\,\mathrm{d}x} = \frac{v_{CNT}\tau_c L_{CNT}}{r} - \frac{2v_{CNT}\tau_c}{r}u(x) \tag{5}$$

This gives the parameters α_p and β_p in Equation (3):

$$\alpha_p = \frac{v_{CNT}\tau_c L_{CNT}}{r} \equiv p_0, \qquad \beta_p = -\frac{2v_{CNT}\tau_c}{r} = -\frac{p_0}{L_{CNT}/2} \tag{6}$$

Introducing this result into Equation (3) and normalizing, the following normalized expression for resistance improvement in steady-state ($\tilde{u} = L_{CNT}/2$) is obtained:

$$\frac{G_{ss}}{G_0} = 1 - \frac{\alpha_p^2}{\beta_p G_0} = 1 + \frac{1}{2}\left(\frac{L_{CNT}}{r}\right)\frac{v_{CNT}\tau_c L_{CNT}}{G_0} \tag{7}$$

The fracture toughness improvement is a function of two dimensionless parameters, the CNT aspect ratio and the energy per unit area of CNT pullout relative to the initial toughness. When the inverse of the aspect ratio is taken as a parameter (see figures in section 'Results and Discussion'), toughness enhancement increases significantly as this parameter approaches zero (nanoscale reinforcement). Significant improvement in toughness is calculated for realistic values of the material and structural parameters, e.g., with 1% CNT volume fraction, 20 μm long CNTs with a diameter of 8 nm, an initial toughness of 200 J/m^2, and an interfacial shear stress of 10 MPa, the toughness would be increased by ~26×. This result is an order of magnitude greater than current experimental data on a 'nanostitched' carbon-fiber prepreg system with these dimensions [18]. Limiting mechanisms of this toughening enhancement are explored in the next section.

CNT Sword-in-sheath Pullout Mechanism

If the maximum stress that is applied to a CNT in the crack wake is higher than its strength, the CNT will fracture. It has been experimentally observed that when MWCNTs fracture, a sword-in-sheath mechanism of failure is observed [32,29,33]. For this process, the energy consumed is reduced from that in the frictional pullout mechanism (section 'Pullout Mechanism') because the IFSS between the outer and the inner CNT ($\tau_{in,out}$) has a value between 0.08 and 0.3 MPa [30], at least two orders of magnitude smaller than the value of the CNT-polymer IFSS [33]. The sword-in-sheath mechanism is similar to the frictional pullout model developed in section 'Pullout Mechanism'. However, apart from the notable difference in IFSS, another difference has been revealed by the tests of Yu et al. [30]. The force necessary to pull the inner CNT out is reduced considerably just prior to

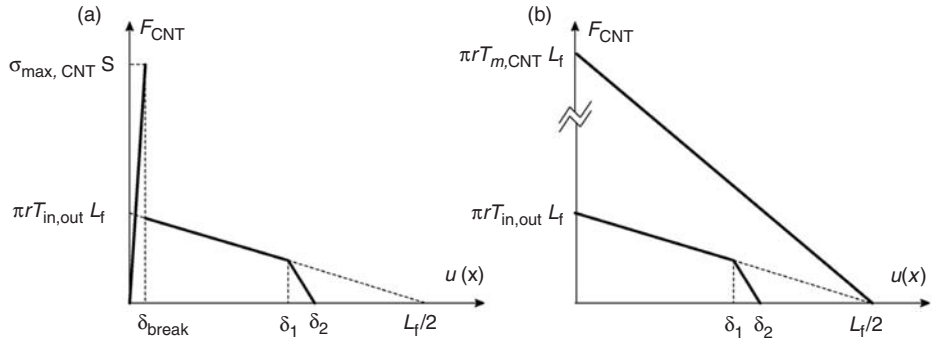

Figure 4. *Mathematical modeling of sword-in-sheath mechanism bridging law. (a) Detailed behavior including CNT elastic deformation and fracture; (b) Mathematical model after neglecting work from CNT breaking. Comparison to CNT-polymer pullout bridging law (not to scale).*

full pullout of the inner CNT from the outer wall. A bridging model extracted from these tests is presented in Figure 4(a).

An analysis of the energy from the CNT breaking process in relation to the energy absorbed by the sword-in-sheath pullout reveals that the associated energy of CNT fracture is negligible, so the model can be simplified to the one shown in Figure 4(b). This is consistent with the interpretation of other authors [22]. The mathematical formulation of the bridging law for the sword-in-sheath pullout mechanism (Figure 4(b)) can be expressed as:

$$p(x) = \begin{cases} \dfrac{2\tau_{\text{in, out}} v_f}{r}\left(\dfrac{L_{CNT}}{2} - u(x)\right) & 0 < u(x) < \delta_1 \\ \dfrac{2\tau_{\text{in, out}} v_f}{r}\dfrac{\dfrac{L_{CNT}}{2} - \delta_1}{\delta_2 - \delta_1}(\delta_2 - u(x)) & \delta_1 < u(x) < \delta_2 \\ 0 & \delta_2 < u(x) \end{cases} \tag{8}$$

where $\delta_1 = (L_{CNT}/2 - \delta_3)$, $\delta_2 = (L_{CNT}/2 - \delta_4)$, and $\delta_3 = 3.5$ μm and $\delta_4 = 2$ μm taken from characteristic values from the Yu et al. tests [30]. With the sword-in-sheath bridging law given above, Equation (7) becomes:

$$\frac{G_{ss}}{G_0} = 1 + \frac{1}{G_0}\left(2\alpha_{ss}\delta_1 + \beta_{ss}\delta_1^2 + \Omega_{ss}(\delta_2 - \delta_1)\right) \tag{9}$$

where

$$\alpha_{ss} = \frac{\tau_{\text{in, out}} v_f L_{CNT}}{r} \qquad \beta_{ss} = -\frac{2\tau_{\text{in, out}} v_f}{r}$$
$$\Omega_{ss} = \frac{\tau_{\text{in, out}} v_f L_{CNT}}{r}\left(1 - \frac{\delta_1}{L_{CNT}/2}\right) \tag{10}$$

This closed-form expression gives us the relative toughening due to sword-in-sheath pullout as a function of the bridging law parameters that is similar to Equation (7). Thus, closed-form expressions for both frictional pullout (Figure 3) and sword-in-sheath sliding/pullout (Figure 4(b)) are available for steady-state toughness enhancement due to bridging fibers of any scale.

RESULTS AND DISCUSSION

In this section, steady-state toughening due to both the pullout and sword-in-sheath mechanisms (Equations (7) and (9)) are, respectively, investigated as a function of the main parameters of the problem. Of particular interest is exploring scale effects on toughness enhancement with aligned reinforcing fibers. Toughening from pullout is shown to be limited by CNT fracture in the crack wake, and combined sword-in-sheath and pullout behavior toughness enhancement curves are subsequently developed.

Steady-state Toughness from Pullout Toughening

The models developed above are used to study parametrically the toughening response of reinforcing fibers, with particular focus on the effect(s) of scale. Comparisons of particular interest focus on differences between the micro (fibers) and the nano (CNTs) scale of reinforcement. Baseline values for all parameters, unless otherwise noted, are: $L_{CNT} = 20\,\mu m$, $r_{CNT} = 4\,nm$, $v_{CNT} = 0.08\%$, $\tau_c = 10\,MPa$, $h = 1.5\,mm$, and $G_{IC} = 200\,J/m^2$. These values are based on the CNT nanostitches produced previously in our group (L_{CNT}, r, and v_{CNT}) [18,34], a conservative value for τ_c [33] and the initiation toughness for an aerospace-grade AS4/8552 (Hexcel) unidirectional tape laminate [18].

The model predicts that reducing the diameter of the stitching fibers from microns (fibers traditionally used to stitch laminates, usually in bundles having diameters of fractions of mm) to nanometers (CNTs) dramatically increases the resistance of the laminate to fracture, i.e., a smaller diameter provides a considerably better reinforcement. This trend and the effect of CNT volume fraction are presented in Figure 5. Higher CNT volume fractions [35], assuming individual CNTs would still pullout, significantly improves the resistance ratio. Here, a conservative value of the friction coefficient

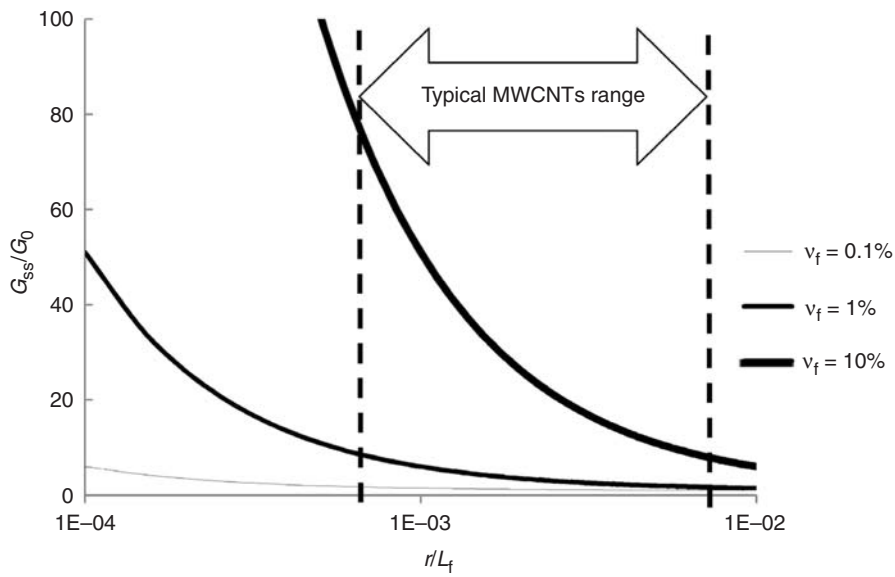

Figure 5. *Effect of the volume fraction. MWCNTs typically have a radius between 4 and 50 nm ($r_f/L = 2 \times 10^{-4}$ to 2.5×10^{-3}). X-axis in logarithmic scale.*

(10 MPa) is used vs. the pullout strength reported for CNTs embedded in a polymer (ranging from 138 MPa obtained through computational simulations [36] to 500 MPa obtained experimentally by Wagner et al. [37]). This yields smaller improvements in toughness as shown in Figure 6 and emphasizes that the identification of this parameter is necessary for the correct interpretation of the CNT bridging mechanism.

Pullout Toughening Limited by CNT Fracture

Large toughness values in the last section lead us to analyze the maximum stress that is applied to each CNT, in order to assess the validity of the pullout model. From Equation (5), the bridging stress has a maximum of p_0 at the crack tip ($x \to 0$; $u \to 0$). The stress on an individual CNT can be calculated based on the bridging traction:

$$\sigma_{\mathrm{CNT,\ max}} = p(x=0)\frac{d^2}{\pi r^2} = \frac{\alpha_p}{v_{\mathrm{CNT}}} = \frac{\tau_c L_{\mathrm{CNT}}}{r} \tag{11}$$

where d is the distance between two adjacent CNTs in a square array. The result of this maximum stress for the example presented at the end of section 'Pullout Mechanism' is 50 GPa. This result is among the highest CNT strength's reported recently [33] for MWCNTs. Limiting pullout toughening based on this criterion is explored in the next section.

Combined Pullout and Sword-in-sheath Steady-state Toughening

The parametric study performed in section 'Steady-state Toughness from pullout Toughening' is limited by the strength of the CNTs (section 'Pullout Toughening

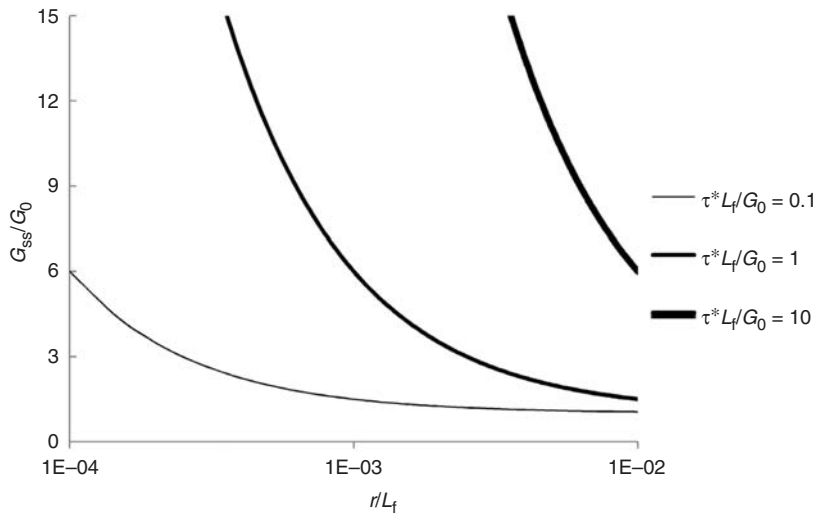

Figure 6. *Effect of interfacial shear stress. MWCNTs typically have a radius between 4 and 5 nm ($r/L_f = 2 \times 10^{-4}$ to 2.5×10^{-3}) and interfacial shear strength between 1 and 100 MPa ($\tau L_f/G_0 = 0.1$ to 10). X-axis in logarithmic scale.*

Limited by CNT Fracture') and completed by considering the sword-in-sheath pullout model (section 'CNT Sword-in-sheath Pullout Mechanism'). If the CNTs fracture, the sword-in-sheath mechanism produces toughening enhancement due to the friction between the inner and outer CNT. The parameters used in this study are the same as in section 'Steady-state Toughness from Pullout Toughening', using a realistic value of $\sigma_{CNT,max} = 30\,GPa$. In Figure 7, the limit of the pullout-mechanism regime is independent of the CNT volume fraction (in agreement with Equation (11)). There is thus a critical fiber aspect ratio that separates the two mechanisms: for the case analyzed $r_{crit} = 6.67\,nm$ ($r_{crit}/L_f = 3.3 \times 10^{-4}$). This value is approximately the radius of the CNTs grown for nanostitching in [18] ($r = 4\,nm$ in that case). Due to the possibility of CNT fracture (Figure 8), it is likely that combinations of these mechanisms are at work. It should be noted that at small nanotube radii (usually they become SWCNT for radii smaller than 2 nm) the sword-in-sheath model is not applicable. In these cases, the SWCNT would fracture completely providing negligible toughness improvement. For a CNT length of 20 μm, this lower limit is below $r/L_f = 10^{-4}$.

As the pullout mechanism consumes more energy than the sword-in-sheath mechanism, CNT fracture is a limiting factor on toughness enhancement when reducing fiber diameter. However, CNT radius is difficult to control from a synthesis standpoint and the easiest way to improve the toughness resistance is to increase the volume fraction of CNTs. As with the pullout mechanism, the same effect of toughness enhancement can be observed for the sword-in-sheath mechanism when the fiber diameter becomes small. In Figure 9, the influence of the CNT-polymer IFSS is presented for its effect on pullout

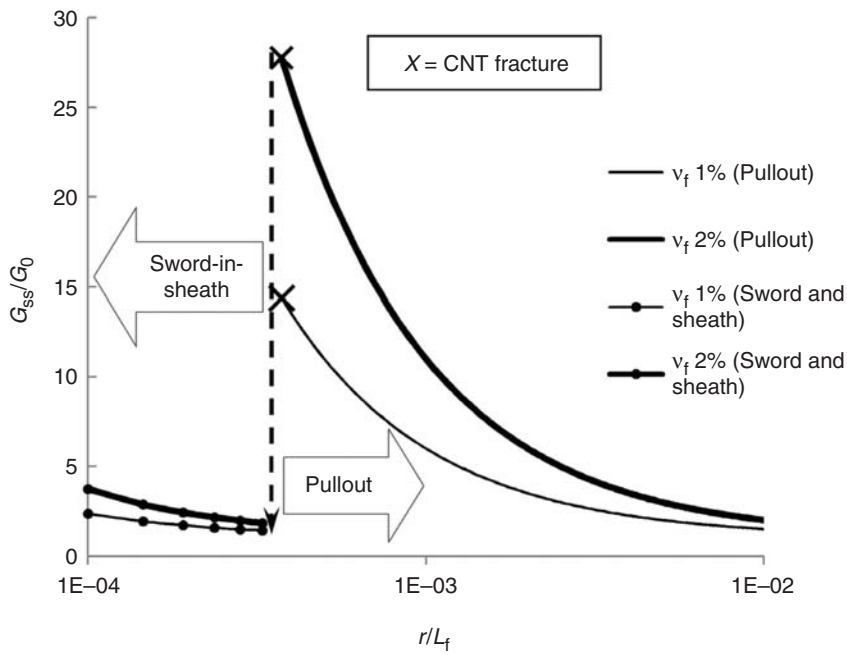

Figure 7. *CNT breakage limitation and influence of volume fraction on sword-in-sheath and pullout mechanisms. In that case, $r_{crit} = 6.67\,nm$ and $r_{crit}/L_f = 3.33 \times 10^{-4}$. MWCNTs typically have a radius between 4 and 50 nm ($r/L_f = 2 \times 10^{-4}$ to 2.5×10^{-3}). X-axis in logarithmic scale.*

mechanism toughening. When the IFSS increases, the pullout toughening maximum moves to higher diameters of bridging fiber due to the CNT fracture criteria, producing CNT breakage and initiating the sword-in-sheath mechanism. CNT length also contributes to limiting pullout toughening, producing earlier breakage. This result

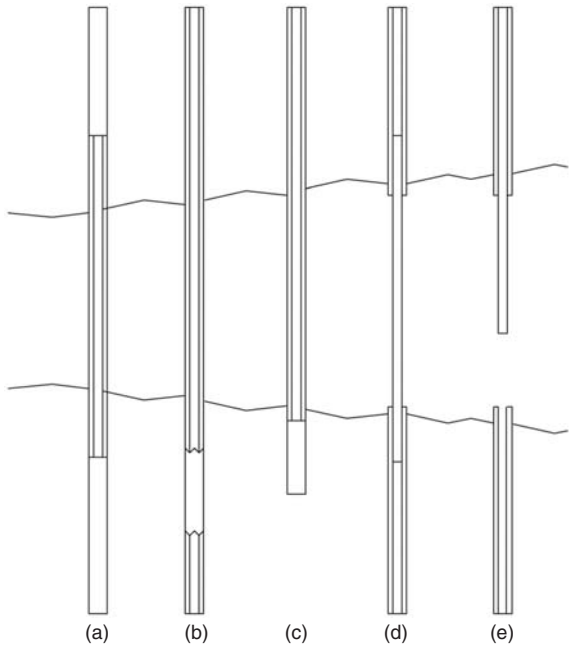

Figure 8. *Other bridging types that can occur compared to ideal pullout (a) and sword-in-sheath (d) mechanisms: partial pullout (b–c) and partial sword-in-sheath (e).*

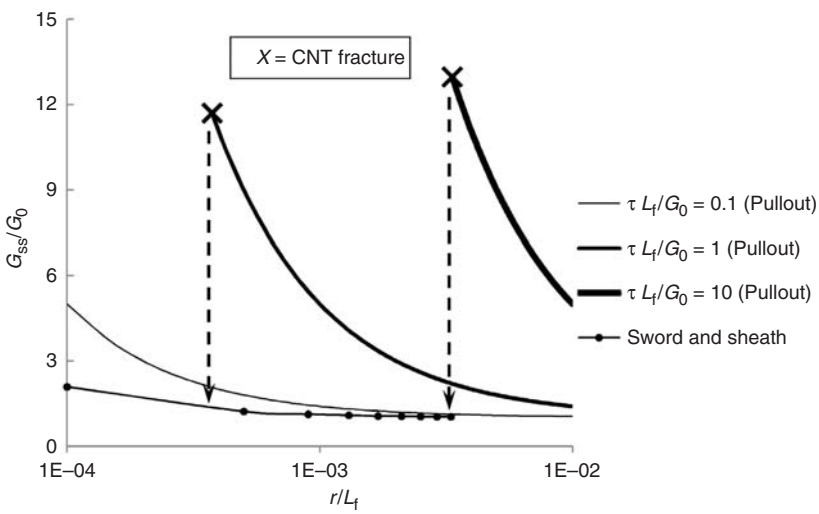

Figure 9. *CNT breakage limitation and influence of the IFSS on sword-in-sheath and pullout toughening mechanisms. MWCNTs typically have a radius of 4 to 50 nm ($r/L_f = 2 \times 10^{-4}$ to 2.5×10^{-3}) and interfacial shear strength between 1 and 100 MPa ($\tau L_f/G_0 = 0.1$ to 10). X-axis in logarithmic scale.*

points out that a tightly packed distribution of short CNTs could give enhanced toughening (e.g., if the parameter r/L_f is maintained at 2×10^{-4}).

FULL R-CURVES FOR MODE I ALIGNED-CNT BRIDGING TOUGHENING

Full analytic R-curves are presented in this section and compared to those from tests of classical pinned [11] and nanostitched [18] laminates.

Closed-form Solution for Full R-curves

A similar approach to that employed in the Jain and Mai Mode I model [38] has been used. They used the exact solution for the stress intensity factor for a DCB proposed by Foote and Buchwald [39] and then calculated the contribution of each pin to the stress intensity factor enhancement and integrated over the bridged zone, obtaining a semi-analytical solution. In our approach, an energetic formulation provides complete analytic solutions. Here, we consider the case of applied moment to cause crack advance (with the usual assumption of ignoring shear deformation), although a point-loaded standard DCB test specimen can be solved in the same way. The condition for crack propagation is that the energy available for creating new surfaces [40] is equal to the critical energy release rate G_0, plus the energy consumed by the CNT bridging:

$$G_R = \frac{12M_c^2}{b^2h^2E} = G_0 + G_{CNT} = G_0 + 2\int_0^{\tilde{u}} p(x)\mathrm{d}u \tag{12}$$

The value of the crack opening before steady-estate ($\tilde{u}$) for a bridged DCB specimen (Figure 2) can be calculated using simple beam theory including the bridging law presented in Equation (2). The result for $\tilde{u}$ is a simple function of the applied moment M_c. Solving the second-order equation that arises by including $\tilde{u}$ in Equation (12), the critical moment (M_c) that causes the crack to propagate as a function of $\Delta\alpha$ is obtained using the pullout and sword-in-sheath bridging laws. Once the critical moment is known, the energy release rate $G_R(\Delta\alpha)$ can be recalculated from the same DCB geometry and applied moment, by removing all the reinforcing fibers. We obtain thus the analytic expression for the R-curve:

$$G_R = \begin{cases} G_R(\Delta\alpha) = \dfrac{12M_c^2}{b^2h^2E} & \text{if} \quad \begin{cases} \tilde{u} < \dfrac{L_{CNT}}{2}\text{(pullout)} \\ \tilde{u} < \delta_1 + \dfrac{\delta_2 - \delta_1}{2}\text{(sword-in-sheath)} \end{cases} \\ G_{ss} = G_R(\Delta\alpha_{ss}) \quad \text{if} \quad \begin{cases} \tilde{u} \geq \dfrac{L_{CNT}}{2}\text{(pullout)} \\ \tilde{u} \geq \delta_1 + \dfrac{\delta_2 - \delta_1}{2}\text{(sword-in-sheath)} \end{cases} \end{cases} \tag{13}$$

The results of this model are validated by comparison with macroscopic z-pinning tests performed by Partidge et al. [11]. Although the z-pins penetrate the entire thickness of the laminate in this case, pullout is produced in one beam of the DCB. The embedded length considered in the equations is therefore half the thickness of the specimen. All the

parameters considered in the analytical mode are: $b = 20\,\text{mm}$, $2h = 3\,\text{mm}$, $v_f = 0.5\%$, $L_f = 1.5\,\text{mm}$, $E = 242\,\text{GPa}$, $r = 0.14\,\text{mm}$, $G_{IC} = 200\,\text{J/m}^2$ and $\tau_c = 30\,\text{MPa}$. These parameters are taken directly from [11] except for the unknown IFSS that has been experimentally observed by other authors, e.g., [41]. The comparison with experimental results in Figure 10 demonstrates that the model can be used to analyze macroscopic z-pin behavior: and nanostitches will be considered next. The z-pin result in Figure 10 for steady-state (~7× enhancement) can be compared with the result that could be obtained if full pullout would appear for CNT reinforcement with the same conditions of IFSS, volume fraction, and G_0. In that case, Equation (7) is only a function of the parameter r/L_f^2 and the results are compared in Figure 11. For a CNT forest with $r = 4\,\text{nm}$ and $L_{CNT} = 20\,\mu\text{m}$, the value of the parameter r/L_f^2 is $\sim 10\,\text{m}^{-1}$ and the fracture toughness enhancement, $G_{ss}/G_0 = 39$. In the case of the z-pinned composite presented as an example, the value of r/L_f^2 is $\sim 62\,\text{m}^{-1}$. The nanoscale effect is significant, providing 6× toughening over the z-pins.

Comparison to Experimental CNT Fracture Toughness Enhancement

The models presented in this work have been compared with recent experimental results presented by our group [18]. In that work, the entire interlaminar space (~20 μm) is bridged with CNTs ($v_f = 1\%$ and $r = 4\,\text{nm}$), giving a fracture toughness enhancement of ($G_{SS}/G_0 \sim 2.5$). The CNT-polymer pullout mechanism toughening predicted from the model presented in section 'Pullout Mechanism' ($G_{SS}/G_0 = 75$) is significantly different than the

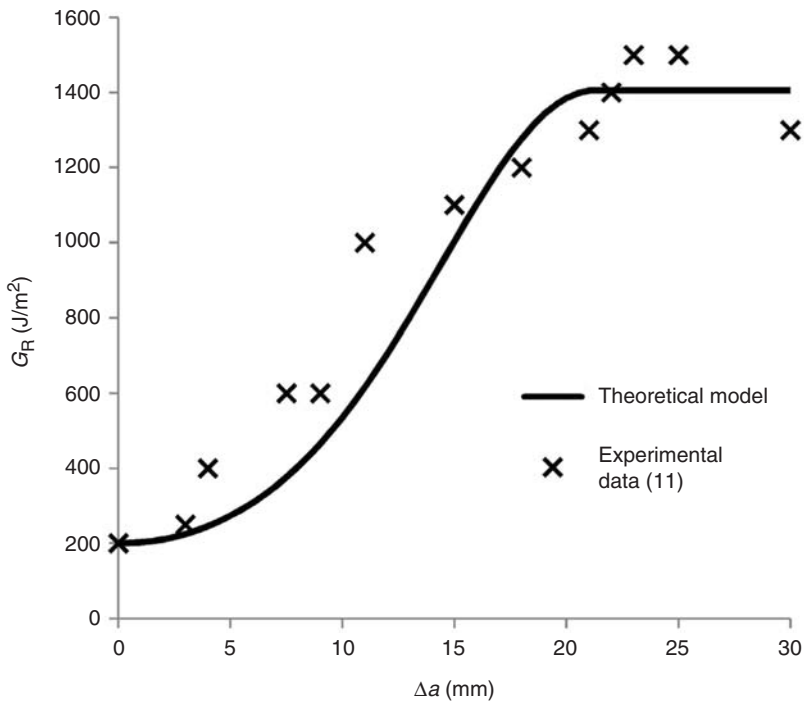

Figure 10. *Z-pinning experimental data [11] and theoretical model comparison.*

experimental results. This suggests that there are other mechanisms at work, and/or combinations of mechanisms (see Figure 8). In Figure 12, the R-curves have been compared for the sword-in-sheath mechanism as well as a 5 μm partial pullout with the same parameters as previous examples and using $\tau_{in,out} = 0.3$ MPa. The comparison indicates that the observed behavior is greater than solely the sword-in-sheath toughening,

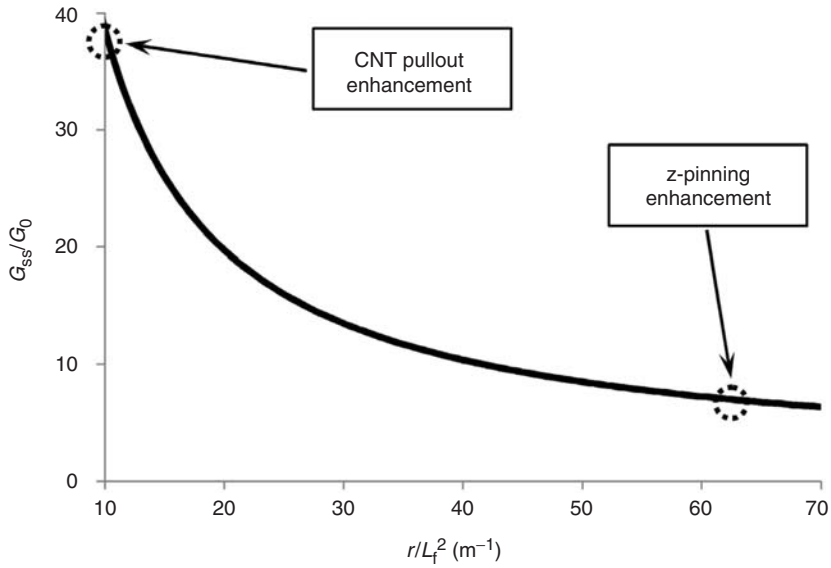

Figure 11. *Fracture toughness improvement for G_0, ν_f, and τ_c constant. In that case, $\nu_f\tau_c/G_0 = 750$, as in [11].*

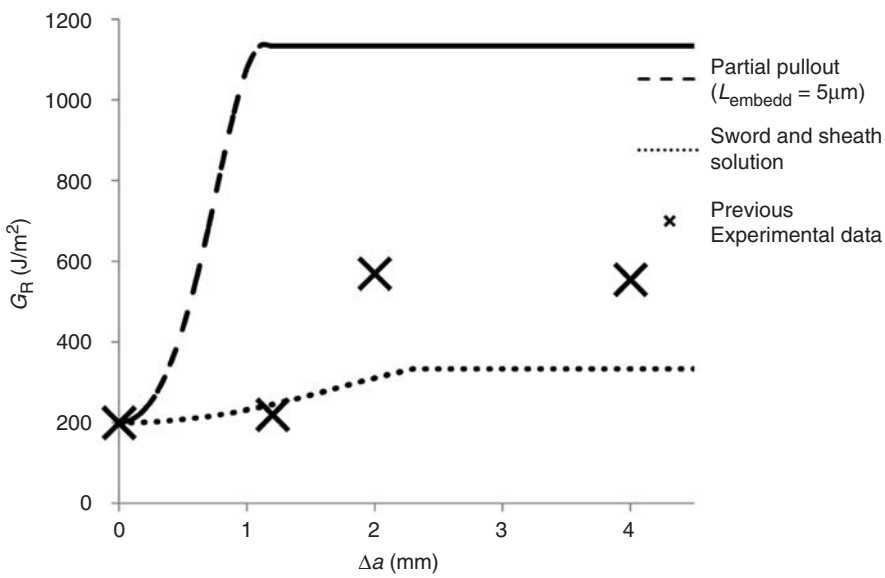

Figure 12. *Complete R-curves for partial pullout ($G_0 = 200$ J/m^2, $L_f = 5$ μm, $\nu_f = 1\%$, $\tau_c = 30$ MPa and $r = 4$ nm) and sword-in-sheath mechanism ($G_0 = 200$ J/m^2, $L_f = 20$ μm, $\nu_f = 1\%$, $\tau_c = 0.3$ MPa and $r = 4$ nm) compared to previous experimental data from [18].*

but less than that expected from partial pullout. In addition to multiple mechanisms being at work, several additional reasons are postulated for the reduced fracture toughness enhancement including fabrication issues affecting assumptions, possible bundling of the MWCNTs during pullout instead of individual pullout, and other differences between experimental conditions and inputs in the models.

CONCLUSIONS

Analytical models that relate key geometric and material parameters to toughness improvement due to reinforcing pins (z-direction fibers) are presented in Mode I bridging problems. Of particular note is the significantly increased toughness predicted as the diameter of the vertically aligned pins approach nanometer dimensions, such as the experimentally realized interlaminar 'nanostitches' reported recently. The mechanisms of frictional pullout of the reinforcing pins, as well as the sword-in-sheath pullout mechanism peculiar to MWCNTs are analyzed in closed form. Toughness improvement is extremely sensitive to CNT aspect ratio, interfacial bonding of the CNTs to the matrix, and CNT volume fraction in steady-state as demonstrated in closed-form in Equation (7). Among the parameters that participate in the bridging process, fiber aspect ratio is critical, with longer stitching fibers allowing a better bridging of the crack. However, high stresses in excess of CNT strength in some cases are present in the bridging zone model at small pin diameters. A stress-based criteria predicts that this effect can limit the toughness improvement from nanoscale reinforcing fibers. The dominant mode(s) of toughening have yet to be elucidated for nanostitched laminates. Extensions or application of the models developed herein to other architectures (such as radially aligned CNTs grown on the surface of advanced fibers) should also be developed. The more realistic case of mixed mode delamination propagation (and conversely toughening) remains to be investigated as well as Mode II loading (preliminary Mode II toughness data indicates 3× improvement over the unreinforced material [18]).

ACKNOWLEDGMENTS

This work was supported by Airbus S.A.S., Boeing, Embraer, Lockheed Martin, Saab AB, Spirit AeroSystems, Textron Inc., Composite Systems Technology, and TohoTenax through MIT's Nano-Engineered Composite aerospace STructures (NECST) Consortium. Enrique Garcia acknowledges support from the La Caixa Foundation, Roberto Guzman de Villoria is grateful for the support of Spain's Ministry of Science and Education (MEC) for the award of a FPU grant (AP-2004-6264), and Joaquin Blanco thanks ISAE-Supaéro for financial support.

REFERENCES

1. Tong, L., Mouritz, A.P. and Bannister, M.K. (2002). *3D Fibre Reinforced Polymer Composites*, Elsevier, Oxford.
2. Poe, C., Reeder, J.R. and Yuan, F.G. (2001). Fracture Behavior of a Stitched Warp-Knit Carbon Fabric Composite, NASA/TM-2001-210868.

3. Glaessgen, E.H., Raju, I.S. and Poe, C.C. (1999). Modeling the Influence of Stitching on Delamination Growth in Stitched Warp-knit Composite Lap Joints, In: *Proceedings of ICCM-12*, Paris, France, Paper No. 449.
4. Glaessgen, E.H. and Raju, I.S. (1999). Three-dimensional Effects in the Plate Element Analysis of Stitched Textile Composites, In: *Proceedings of the 40th AIAA/ASME/ASCE/AHS/ASC Structures, Structural Dynamics, and Materials Conference and Exhibit St. Louis*, Missouri, AIAA-99-1416.
5. Stickler, P.B. and Ramulu, M. (2001). Investigation of Mechanical Behaviour of Transverse Stitched T-joints with PR520 Resin in Flexure and Tension, *Composite Structures*, **52**: 307–314.
6. Stickler, P.B. and Ramulu, M. (2002). Parametric Analyses of Stitched Composite T-joints by the Finite Element Method, *Materials and Design*, **23**: 751–758.
7. Stanley, L.E. and Adams, D.O. (2001). Development and Evaluation of Stitched Sandwich Panels. NASA/CR-2001-211025.
8. Krueger, R. and O'Brien, T.K. (2000). A Shell/3D Modeling Technique for the Analysis of Delaminated Composite Laminates, NASA-2000-TM210287.
9. Dransfield, K.A., Jain, L.K. and Mai, Y.W. (1998). On the Effects of Stitching in CFRPs—I. Mode I Delamination Toughness, *Computer Science and Technology*, **58**: 815–827.
10. Jain, L.K., Dransfield, K.A. and Mai, Y.W. (1998). On the Effects of Stitching in CFRPs—II. Mode II Delamination Toughness, *Computer Science and Technology*, **58**: 829–837.
11. Partridge, I.K. and Cartié, D.D.R. (2005). Delamination Resistant Laminates by Z-Fiber® Pinning: Part I Manufacture and Fracture Performance, *Composites Part A*, **36**(1): 55–64.
12. Mouritz, A.P., Leong, K.H. and Herszberg, I. (1999). A Review of the Effect of Stitching on the In-plane Mechanical Properties of Fibre-reinforced Polymer Composites, *Composites Part A*, **28**: 979–991.
13. Steeves, C.A. and Fleck, N.A. (2006). In-plane Properties of Composite Laminates with Through-thickness Pin Reinforcement, *International Journal of Solids and Structures*, **43**: 3197–3212.
14. Kim, Y.A., Kamio, L., Tajiri, T., Hayashi, T., Song, S.M., Endo, M., Terrones, M. and Dresseslhaus, M.S. (2007). Enhanced Thermal Conductivity of Carbon Fiber/Phenolic Resin Composites by the Introduction of Carbon Nanotubes, *Applied Physics Letters*, **90**: 093125.
15. Bekyarova, E., Thostenson, E.T., Yu, A., Kim, H., Gao, J., Tang, J., Hahn, H.T., Chou, T.-W., Itkis, M.E. and Haddon R.C. (2007). Multiscale Carbon Nanotube-Carbon Fiber Reinforcement for Advanced Epoxy Composites, *Langmuir*, **23**(7): 3970–3974.
16. Adhikari, K., Hubert, P., Simard, B. and Johnston, A. (2006). *Proc. 47th AIAA/ASME/ASCE/AHS Conference*, Newport, R.I., AIAA-2006-1855-604.
17. Thakre, P.R., Lagoudas, D.C., Zhu, J. and Barrera, E.V. (2006). *Proc. 47th AIAA/ASME/ASCE/AHS Conference*, Newport, R.I. AIAA-2006-1857-212.
18. Garcia, E.J., Wardle, B.L. and Hart, A.J. (2008). Joining Prepreg Composite Interfaces with Aligned Carbon Nanotubes, *Composites: Part A*, **39**: 1065–1070.
19. Cooper, C.A., Cohen, S.R., Barber, A.H. and Wagner, H.D. (2002). Detachment of Carbon Nanotubes from a Polymer Matrix, *Applied Physics Letters*, **81**(20): 3873–3875.
20. Barber, A.H., Cohen, S.R. and Wagner, H.D. (2003). Measurement of Carbon Nanotube-Polymer Interfacial Strength, *Applied Physics Letters*, **82**(23): 4140–4142.
21. Dai, S.-C., Yan, W., Liu, H.-Y. and Mai, Y.W. (2004). Experimental Study on Z-Pin Bridging Law by Pullout Test, *Composites Science and Technology*, **64**(16): 2451–2457.
22. Tong, L., Tan, P. and Sun, X. (2008). Effect of Long Multi-walled CNTs on Delamination Toughness of Laminated Composites, *Journal of Computation and Mathematics*, **42**: 5–23.
23. Lindhagen, J.E. and Berglund, L.A. (2000). Application of Bridging-law Concepts to Short-fibre Composites. Part I: DCB Test Procedures for Bridging Law and Fracture Energy, *Composites Science and Technology*, **60**: 871–883.
24. Sorensen, L., Botsis, J., Gmür, Th. and Humbert, L. (2008) Bridging Tractions in Mode I Delamination: Measurements and Simulations, *Composites Science and Technology*, **68**: 2350–2358.

25. Veedu, V.P., Cao, A., Li, X., Ma, K., Soldano, C., Kar, S., Ajayan, P.M. and Ghasemi-Nejhad, M. (2006). Multifunctional Composites Using Reinforced Laminae with Carbon-nanotube Forests, *Nature Materials*, **5**: 457–462.
26. Garcia, E.J., Wardle, B.L. and Hart, A.J. (2008). Fabrication and Multifunctional Properties of a Hybrid Laminate with Aligned Carbon Nanotubes Grown In Situ, *Composites Science and Technology*, **68**: 2034–2041.
27. Suo, Z., Bao, G. and Fan, B. (1992). Delamination R-Curve Phenomena Due to Damage, *Journal of Mechanics and Physics of Solids*, **40**(1): 1–16.
28. Rice, J.R. (1968). A Path Independent Integral and the Approximate Analysis of Strain Concentration by Notches and Cracks, *Journal of Applied Mechanics*, **35**(2): 379–386.
29. Ruoff, R.S., Calabri, L., Ding, W. and Pugno, N.M. (2005). Experimental Tests on Fracture Strength of Nanotubes, *Reviews on Advanced Materials Science*, **10**: 110–117.
30. Yu, M.F., Yakobson, B.I. and Ruoff, R.S. (2000). Controlled Sliding and Pullout of Nested Shells in Individual Multiwalled Carbon Nanotubes, *The Journal of Physical Chemistry B*, **104**(37): 8764–8767.
31. Dugdale, D.S. (1960). Yielding of Steel Sheets Containing Sleets, *Journal of Mechanics and Physics of Solids*, **8**: 100–104.
32. Hwang, G.L., Shieth, Y.T. and Hwang, K.C. (2004). Efficient Load Transfer to Polymer Grafted Multiwalled Carbon Nanotubes in Polymer Composites, *Advanced Functional Materials*, **14**(5): 487–491.
33. Coleman, J.N., Khan, K., Blau, W.J. and Yurii, K.J. (2006). Small but Strong: A Review of the Mechanical Properties of Carbon Nanotube-polimer Composites, *Carbon 44*, 1624–1652.
34. Garcia, E.J., Hart, J. and Wardle, B.L. (2008). Long Carbon Nanotubes Grown on the Surface of Fibers for Hybrid Composites, *AIAA Journal*, **46**(6): 1405–1412.
35. Wardle, B.L., Saito, D.S., Garcia, E.J., Hart, A.J. and Guzman de Villoria, R. (2008). Fabrication and Characterization of Ultra-high Volume Fraction Aligned Carbon-nanotube-polymer Composites, *Advanced Materials*, **20**: 2707–2714.
36. Wong, M., Paramsothy, M., Xu, X.J., Ren, Y, Li, S. and Liao, K. (2004). Physical Interactions at Carbon Nanotube–polymer Interface, *Polymer 44*, **25**: 7757–7764.
37. Wagner, H.D., Lourie, O., Feldman, Y. and Tenne R. (1998). Stress-induced Fragmentation of Multiwall Carbon Nanotubes in a Polymer Matrix, *Applied Physics Letters*, **72**(2): 188–190.
38. Jain, L.K. and Mai, Y.W. (1994). Mode I Delamination Toughness of Laminated Composites with Through-thickness Reinforcement, *Applied Composite Materials*, **1**(1): 1–17.
39. Foote, R.M.L. and Buchwald, V.T. (1984). An Exact Solution for the Stress Intensity Factor for a Double Cantilever Beam, *International Journal of Fracture*, **29**: 125–134.
40. Anderson, T.L. (1995). *Fracture Mechanics: Fundamentals and Applications*, CRC Press, London.
41. Reed, R.P. and Berg, J.C. (2006). Measuring Effective Interfacial Shear Strength in Carbon Fiber Bundle Polymeric Composites, *Journal of Adhesion Science and Technology*, **20**(16): 1919–1936.